ARL-TR-8582 ● Nov 2018

US Army Research Laboratory

Atmospheric Renewable Energy Research, Volume 6: Atmospheric Renewable Energy Field Study No. 3 and Preparation for Tactical Power In-situ Atmospheric Intelligence

by Gail Vaucher and Andrew Welch

NOTICES

Disclaimers

The findings in this report are not to be construed as an official Department of the Army position unless so designated by other authorized documents.

Citation of manufacturer's or trade names does not constitute an official endorsement or approval of the use thereof.

Destroy this report when it is no longer needed. Do not return it to the originator.

ARL-TR-8582 ● NOV 2018

US Army Research Laboratory

Atmospheric Renewable Energy Research, Volume 6: Atmospheric Renewable Energy Field Study No. 3 and Preparation for Tactical Power In-situ Atmospheric Intelligence

by Gail Vaucher
Computational and Information Sciences Directorate, ARL

Andrew Welch
Reserve Officers' Training Corps Internship, University of Nevada–Reno

REPORT DOCUMENTATION PAGE

Form Approved
OMB No. 0704-0188

1. REPORT DATE *(DD-MM-YYYY)*	2. REPORT TYPE	3. DATES COVERED (From - To)
November 2018	Technical Report	14 May 2018–30 September 2018

4. TITLE AND SUBTITLE
Atmospheric Renewable Energy Research, Volume 6: Atmospheric Renewable Energy Field Study No. 3 and Preparation for Tactical Power In-situ Atmospheric Intelligence

5a. CONTRACT NUMBER

5b. GRANT NUMBER

5c. PROGRAM ELEMENT NUMBER

6. AUTHOR(S)
Gail Vaucher and Andrew Welch

5d. PROJECT NUMBER

5e. TASK NUMBER

5f. WORK UNIT NUMBER

7. PERFORMING ORGANIZATION NAME(S) AND ADDRESS(ES)
US Army Research Laboratory
Computational and Information Sciences Directorate:
Battlefield Environment Division (ATTN: RDRL-CIE-D)
White Sands Missile Range, NM 88002-5501

8. PERFORMING ORGANIZATION REPORT NUMBER
ARL-TR-8582

9. SPONSORING/MONITORING AGENCY NAME(S) AND ADDRESS(ES)

10. SPONSOR/MONITOR'S ACRONYM(S)

11. SPONSOR/MONITOR'S REPORT NUMBER(S)

12. DISTRIBUTION/AVAILABILITY STATEMENT
Approved for public release; distribution is unlimited.

13. SUPPLEMENTARY NOTES

14. ABSTRACT
Tactical power independence is strengthened with the hybridizing of solar energy into a tactical power-grid design. To optimize such a hybrid grid performance, knowledge of current and future atmospheric contributions is critical. The Atmospheric Renewable Energy Field Study no. 3 (ARE3) promotes this quest by furthering the acquisition of novel and detailed power, solar radiation, and cloud/sky documentation data. These data also serve as a resource toward the development of a solar radiation flux model that will provide atmospheric intelligence for future tactical power grids. In this report, a sample of the solar radiation models surveyed for hybrid power applications is presented, along with the identification of a "best fit" model that satisfies the current tactical energy unit independence requirements. Balanced and unbalanced power grid conditions are graphically displayed as a sample product of the preliminary ARE3 data analysis. The ARE3 data acquired and analyzed continue to advance the US Army Research Laboratory toward a better understanding of the atmospheric influences upon the hybrid power grids utilizing solar energy, as well as toward the creation of a smart (atmospherically informed) tactical hybrid power grid.

15. SUBJECT TERMS
atmospheric renewable energy, ARE3, hybrid power, solar radiation, simulated Whole Sky Imager, sWSI, Power Train

16. SECURITY CLASSIFICATION OF:			17. LIMITATION OF ABSTRACT	18. NUMBER OF PAGES	19a. NAME OF RESPONSIBLE PERSON
a. REPORT	b. ABSTRACT	c. THIS PAGE			Gail Vaucher
Unclassified	Unclassified	Unclassified	UU	46	19b. TELEPHONE NUMBER (Include area code) (575) 678-3237

Contents

List of Figures

List of Tables

Acknowledgments

The authors wish to thank Sean D'Arcy for his work in maintaining the Power Train, Robert Brice for his help with the pyranometer setup, and Dr Patrice Collins and her Outreach Office colleagues for their work in providing a Reserve Officers' Training Corps Internship program. Also, special thanks go to the Technical Publishing Branch for its technical-editing excellence, specifically to Jessica Schultheis (supervisor) and Martin Kufus (editor).

Executive Summary

Uninterrupted electrical power is critical for tactical readiness, especially in supporting the armed services decisive overmatch strategies. General applications for this research include, but are not limited to, long-range precision fires; next-generation combat vehicles; future vertical lifts; network command, control, communications, and intelligence; and air and missile defenses, as well as the creation of synthetic training environments for future Soldiers. In short, all missions that depend upon consistent, reliable electrical power.

Progressive strengthening of tactical power resources through diversity and the integration of renewable energy were initiated with the Public Law 109–58 *Energy Policy Act of 2005*.[1] While there are many types of renewable energy, this research focuses on solar energy. The strategy of integrating solar has evolved over the last decade, from a replacement resource to a supplemental power source for a hybridized power grid. The atmospheric impact on such a hybrid grid is the focus of this US Army Research Laboratory (ARL) research. Atmospheric solar energy forecasting for the national solar power microgrids has provided useful experiences from which ARL has extracted lessons learned for tactical applications. Timeliness and the need for energy independence severely limit the immediate transference of solar energy forecast models into the tactical power grid functions. Consequently, after describing the 2018 Atmospheric Renewable Energy Field Study no. 3 (ARE3), a chapter captures a sample of the solar radiation models considered for tactical hybrid power applications. With a model identified as tactically relevant, the ongoing challenges of satisfying the model input requirements are described.

Examples of the ARE3 preliminary field study results are given. Starting with the multiple-sensor time stamp alignments, power data checks reveal consistent time series patterns generated by the three power types sampled: Photovoltaic (PV), Battery and Load Powers. The "non-noisy" ARE3 Power time series and the close magnitudes between the PV and "Battery + Load" Powers, demonstrate significant improvement in the Power Train design and the informative potential of the Power data. The edifying examples of ARE3 Power and atmospheric parameter time series include balanced and unbalanced power grid conditions. Both states have been examined. Visualizations of the ARE3 power and atmospheric data are presented in daily midnight-to-midnight graphics.

In summary, the July 2018 ARE3 data and ongoing analyses continue to advance ARL toward a better understanding of the atmospheric influences upon the hybrid

[1] United States Congress. Public law 109–58. Energy policy act of 2005. Washington (DC): Government Printing Office (US). 2005 Aug 8.

power grids utilizing solar energy. Coupling this dataset with the identification of a tactically relevant solar radiation model exhibits significant progress toward the creation of a smart (atmospherically informed) tactical hybrid power grid.

1. Introduction

Successful tactical readiness depends on reliable, uninterrupted power. This "power" is not only referring to capabilities supporting the armed services' decisive overmatch strategies, but an even more basic definition of "power"— electrical power. Electrical power enables all non-kinetic driven devices both on and off the battlefield. The ability to consistently and smartly produce and optimize this electrical power through a cost-effective method is the central focus of the research. General applications for this research include, but are not limited to, long-range precision fires; next-generation combat vehicles; future vertical lifts; network command, control, communications, and intelligence; and air and missile defenses, as well as the creation of synthetic training environments for future Soldiers. In short, all missions that depend upon consistent, reliable electrical power.

History: With Public Law 109–58 *Energy Policy Act of 2005* (US Congress 2005), the armed services committed themselves to the integration of renewable energies. A Presidential Mandate in 2013 solidified this commitment by agreeing to convert 20% of the Department of Defense (DOD) energy into renewable energy resources by 2020. Complementing the vision, the DOD established a Directive (no. 4180.01) to enhance military capabilities, improve energy security and mitigate energy usages and management costs. The integration of renewable energy resources was one method for fulfilling the Directive. The challenge, however, was in the details **(**Vaucher 2015).

Renewable Energy: There are numerous renewable energy resources, such as solar, wind, water, nuclear, and geothermal. Due to the mobility requirements of the US armed forces, the list was quickly reduced to the Navy's nuclear-powered vessels, the use of biofuels—such as those used by the Air Force for their jets—and the possible use of solar and wind energy in Forward Operating Base scenarios. As economics and logistics were considered, solar (and wind) energy remained a viable nontraditional power-generating alternative and is the focus of this study.

Tactical Solar Energy: One of the initial responses to the introduction of solar energy into the tactical world was to have this new energy resource replace the traditional power-generating devices (namely, generator and battery). Since the solar energy is only available during daytime hours, and can be further challenged when objects (such as clouds) block solar rays from reaching the technology needed to convert sunshine into useful electrical power, the one-to-one replacement option was hardly realistic. Consequently, a mix of traditional and nontraditional power generating resources, "hybrid" power was considered.

Atmospheric Forecasting for National Grid Solar Energy: For solar energy to be effectively integrated into a hybrid power grid, understanding and exploiting the atmospheric influence on solar energy materials was the next step. This step began by investigating the process of designing solar power resources and testing the results on applications such as meteorological towers used for US Army Research Laboratory (ARL) field studies. (Vaucher 2016a). Concurrently investigated were atmospheric forecasting techniques being developed by various universities and agencies for the national solar energy power grids. The primary atmospheric parameter needed by the power grid community was solar radiation. The diverse atmospheric forecasting approaches that were being developed for the national power grids framed the methods ARL considered for a tactical environment. A sample of these methods includes the following (Haupt et al. 2016):

- Statistical Forecasting, which is based on regime-dependent artificial intelligence forecasting techniques utilizing pyranometer* data measured at a given location as well as concurrent meteorological observations and forecasts.
- Multisensor Advection Diffusion NowCast (MADCast), which is a satellite-based model that integrates 3-D cloud pictures based on multiple satellite images and profilers into the dynamic core of Weather Research and Forecasting (WRF). MADCast was also designed for the analysis and short-term forecasting of clouds (Auligné 2014a, 2014b; Descombes et al. 2014).
- Total Sky Imager Forecast, which operates with a timescale of only a few minutes to approximately 15 min. The project identified technology able to discriminate cloud levels and discern cloud advection according to the winds observed at those levels. Improvements over "smart persistence" were about 29% for the short-term forecasts.
- Cooperative Institute for Research in the Atmosphere Forecast (CIRACast), which is a cloud-motion system that advanced cloud shadowing, removed parallax, and implemented better advecting winds at different altitudes than its predecessor. CIRACast showed a 25%–40% improvement over Smart Persistence.
- WRF-Solar, which provided the first numerical weather prediction model specifically designed to meet the needs of irradiance forecasting. This model accounted for deviations associated with the eccentricity of the

* A pyranometer is a research-grade sensor that measures the solar intensity coming from both direct solar radiation and diffuse sky radiation (AMS 2012).

Earth's orbit and the obliquity of the Earth; it included the direct normal irradiance and diffuse solar radiation components from the radiation parameterization; and had efficient parameterizations. WRF-Solar was developed to improve the representation of absorption and scattering of radiation by aerosols (aerosol direct effect); included aerosols interacting with cloud microphysics, altering the cloud evolution and radiative properties, an effect that had been traditionally only implemented in atmospheric computationally costly chemistry models. It included feedback that subgrid scale clouds produced in shortwave irradiance as implemented in a shallow cumulus parameterization; allowed the assimilation of infrared irradiances from satellites to determine the 3-D cloud field, and allowed for an improved initialization of the cloud field that increased the performance of short-range forecasts. WRF-Solar improved clear sky irradiance prediction by 15%–80% over a standard version of WRF, depending on location and cloud conditions.

Two attributes of the atmospheric models reviewed significantly limited their direct implementation into the tactical application: 1) most atmospheric forecast models required large datasets accessed over public networks, as well as 2) significant computing power. To establish and maintain a decisive tactical overmatch against aggressors, military power resources need to operate with tactical energy unit independence. Thus, neither attribute supports the requirement for independence.

Tactical Microgrids: In Vaucher et al. (2016), ARL explored tactical microgrids. Beginning with traditional tactical microgrid data from a Base Camp Integration Laboratory demonstration, a simulation of a future hybrid microgrid was created. Results from the simulations confirmed that lower fossil-fuel consumption resulted when the nontraditional solar energy resources were integrated. It was also discovered that the accuracy of the weather forecast had a significant impact in the hybrid's efficiency (Parker 2018).

Consequently, ARL pursued a method for supporting future hybrid-power resources using in-situ only meteorological information. Two ARL technical reports (Vaucher et. al 2017; Walker and Vaucher 2017) document the initial milestones crossed toward this goal. In this technical report, additional materials provide greater depth toward the objective, paving the way for constructing a "proof of concept" in-situ atmospheric intelligence technology.

2. Atmospheric Renewable Energy (ARE) Field Studies

The ARE field studies were designed as a data-generating resource for researching the atmospheric influences on solar energy. As explained in ARE Research, Volume 3 (Vaucher et al. 2016), the primary atmospheric parameters associated with solar energy are solar radiation and ambient temperature. The solar energy that enters the earth's atmosphere from space is generally considered a constant (1,367 W/m^2). For this research, the technology converting solar energy into electrical power is a photovoltaic (PV) panel. The greatest inhibitors of solar radiation completing its trek from space to the PV panel mounted on the earth's surface are hard and soft shadows. Examples of hard shadows would be shade cast by building structures, fallen branches, growing plants, and so on. Soft shadow examples include shadows cast by clouds, aerosols, and dust. Since most hard shadows can be mitigated through design/configuration choices, the field studies focused on quantifying the soft shadows. An elaboration of this topic will be given in Section 3.

Ambient temperatures impacting solar power generation primarily impact PV system efficiency. As per Boxwell's observations, the ambient temperature used for the PV panel calibration of "peak power" is 25 °C. For every 1 °C above (or below) the calibration ambient temperature, the solar power system will lose (or gain) a 0.5% efficiency (Boxwell 2013). Consequently, a system's efficiency drops when temperatures are extremely warm. When temperatures are colder, efficiency improves with respect to the panel's peak power.

2.1 ARE Field Study No. 2 and No. 3

The ARE Field Study no. 2 (ARE2) and ARE Field Study no. 3 (ARE3) were conducted during the summer months from the roof of a two-story building at White Sands Missile Range, New Mexico. ARE2 began on 2017 June 16 and ended on 2017 August 14. ARE3 was initiated on 2018 July 24 and ended on 2018 July 30. The underlying goal was to capture a variety of clear, partly cloudy, and overcast sky conditions. As the monsoon season occurs during the summer months in southern New Mexico, this objective was easily met.

The ARE Southwestern USA desert field location was situated on the west side of an approximately 40-mile-wide, relatively flat basin. A relatively flat mountain ridge rising about 10,000 ft mean sea level (MSL) lined the east side of the Tularosa Basin. On the northeast slopes of that ridge was a single mountain peak of 12,000 ft MSL. The west side mountain ridge was jagged, rising about 8,000 ft MSL.

2.2 Major Elements of the ARE Field Design

The ARE2 and ARE3 field designs consisted of three major elements: a Power Train, in-situ atmospheric measurements, and regional weather summaries.

2.2.1 Power Train

The Power Train consisted of four major elements, as shown in Fig. 1: the PV panel, controller, batteries, and a digital load. Current and voltages were sampled at three locations, then used to calculate power. PV Power was sampled between the PV panel and controller. Battery Power used current and voltages measured between the controller and battery. Load Power was calculated from current and voltage data acquired between the controller and load.

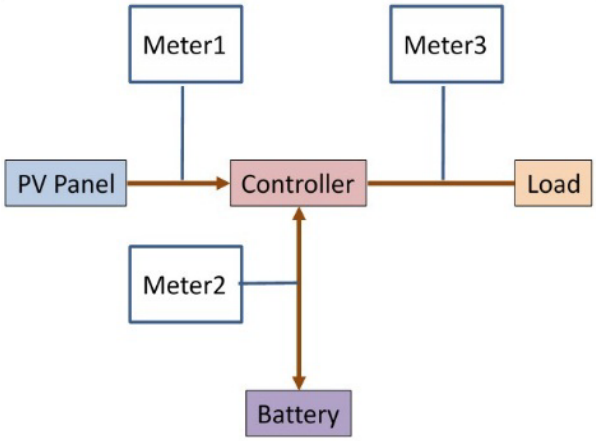

Fig. 1 ARE2 Power Train major elements (Vaucher et al. 2017)

While two physically different PV panels were used for ARE2 and ARE3, the hardware design and specifications were consistent: The single solar PV panel was a 72-cell SolarWorld (Sunmodule SW 315 XL Mono) that faced south and was tilted at an angle of about 32°, the approximate latitude of the site.* The panel had a rated maximum power of 315 W (–0/+5Wp) and a maximum system voltage of 1000 V DC. The rated voltage was 36.8 V and the rated current was 8.63 A.

The solar energy generated from the PV panel was managed by a 30-A Maximum Power Point Tracking (MPPT) Charge Controller (MidNite Solar, Model "the Kid"). Four Trojan T105re (renewable energy) deep-cycle flooded lead acid batteries were charged by the controller, using the PV panel output. A BK Precision 8510 Programmable DC Electronic (Digital) Load balanced the electrical flow in the ARE2 and ARE3 Power Trains.

* Optimum solar-photon intake occurs when photons arrive orthogonally (at 90°) to the PV plane (Vaucher 2016). Thus, the PV panel was oriented at the local latitude angle.

The batteries absorbed or discharged power, depending on whether the PV panel was generating electricity. The Digital Load absorbed power, simulating an electrically powered application. Power was regulated between the battery and load via the MPPT controller. Manual adjustments to the Digital Load ensured a balanced distribution of electrical power. As per Volume 4 (Vaucher et al. 2017), the ideal Load values were greater than 22 V in the morning, and less than 25 V in the evening. When morning voltage dropped below 22 V, the Load amperage was reduced to let the batteries charge. When the evening voltage exceeded 25 V, the Load was increased, which then brought the voltage down. As will be described in Section 4.3, when the power train was successfully "balanced" (optimized for power distribution), the current time series imitated the same graphical shape of the solar radiation intake (time series).

2.2.2 In-situ Atmospheric Measurements

The local ARE atmospheric conditions were documented with measurements taken by the Local-Rapid Evaluation of Atmospheric Conditions (L-REAC) System, located approximately 16 m north of the ARE field site (Fig. 2). This tripod of meteorological sensors included two temperatures sensors sampling at 5.7 m and 0.7 m above roof level (ArL) as well as a zenith-facing pyranometer that quantified the solar radiation at 2 m ArL. Other atmospheric parameters concurrently sampled consisted of pressure (1 m ArL), relative humidity (2 m ArL), and wind speed/direction (6 m ArL). Measurements were sampled every 10 s and reduced to 1-min averages. (For more detailed information, see L-REAC System (Vaucher et al. 2011.)

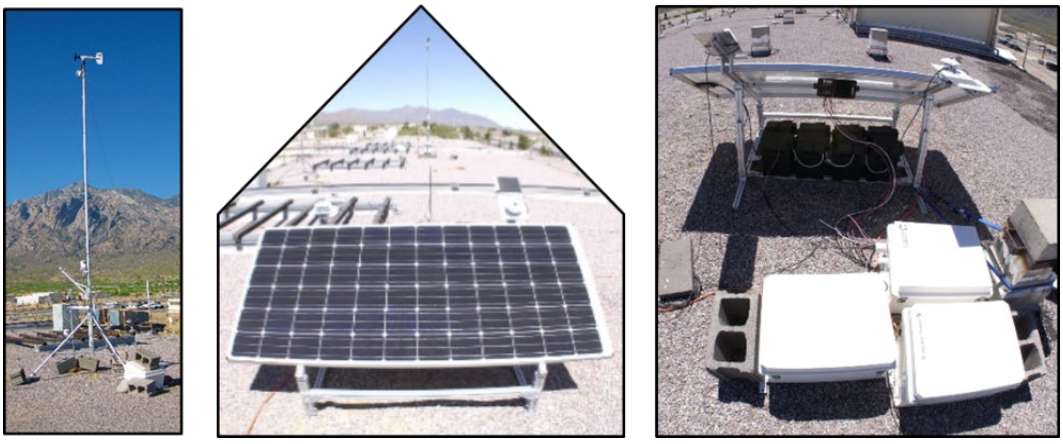

Fig. 2 L-REAC and ARE2 systems: The L-REAC system is in the left and central images and ARE2 system is in the central and right images; in the right image, the zenith facing pyranometer is on the right (west) side and the pyranometer aligned with the angled PV is on the left (east) side.

2.2.2.1 ARE Solar Radiation

ARE2 and ARE3 in-situ solar radiation measurements were taken by two Kipp and Zonen Model CM3 pyranometers sampling every 10 s in W/m^2 and calculating 1-min average outputs. Each pyranometer was mounted on a flat plate that was attached to the top of the PV panel (see Fig. 2). Pyranometer (no. 1)–West was mounted in a zenith-facing orientation on the northwest corner of the PV panel (about 1.05 m ArL). Pyranometer (no. 2)–East was attached to the northeast corner of the PV panel and angled at approximately 32°, the same angle as the PV panel. The Pyranometer–East height was about 1.03 m ArL. As explained in Vaucher et al. 2017, the angled perspective reported higher magnitudes of solar energy during the mid-day hours than the zenith-facing sensor.

2.2.2.2 Sky Documentation

Sky documentation required three steps: acquiring an image from a simulated Whole Sky Imager (sWSI), logging cloud observations within minutes of the sWSI image, and extracting online, automated observations from nearby weather resources (see Section 2.2.3).

In both ARE2 and ARE3, the sWSI used was a Professional Nikon D750 camera with a Sigma 8-mm, 180° fisheye lens. The sky observations followed a standard three-tiered (low, middle, and high layer) sky observation process that included cloud types and amounts. An elaboration of the method for documenting the sky/cloud conditions will be described in Section 3.

2.2.3 Regional Weather Summaries

For post-ARE analyses, weather summaries from climatologically-derived upwind, onsite, and downwind regional locations captured the current and forecasted weather events of the area. The upwind location was from the National Weather Service, El Paso, Texas–Santa Teresa, New Mexico site, which was southwest of the 8,000-ft-tall (MSL) western ridge. The daily weather discussion issued from White Sands Weather Forecast Office at White Sands Missile Range captured the onsite perspective. An automated weather sensor at the Holloman Air Force Base, within 40 miles northeast of the ARE field site, provided a downwind description.

3. Real-Time Solar Radiation Assessment

The optimization of solar energy in a hybrid power grid comes, in part, from exploiting the known and anticipated atmospheric conditions. The current solar energy resources can be determined with research-grade sensors called, pyranometers.

In a tactical environment, the cost and maintenance requirements of such sensors (such as, routine calibration) are not practical. Consequently, this research pursued the use of a solar radiation model that had minimal input requirements and was both cost effective and tactically securable. In the following sections, we present a sample of results from a solar radiation model survey, along with subsequent research and development actions.

3.1 Solar Radiation Model Survey

Two independent surveys were conducted for a model capable of calculating atmospheric parameters relevant to the local solar power generation. Since the application of this model is for an isolated scenario (tactical energy unit independence), model input and computational requirements were restricted to just in-situ resources. This attribute automatically eliminated most contemporary atmospheric models, causing the survey to focus on methods published during the 1980–2000 time period. The model selected for additional investigation would also need to complete all data processing within seconds to ensure timely and relevant intelligence.

A sample of the various models identified is provided in Table 1. These include the following:

- SOLARFLUX: The SOLARFLUX model is a Geographic Information System (GIS)-based solar irradiance model that calculates solar insolation for complex topography based on surface orientation, solar angle, horizon shading, and atmospheric attenuation (Hetrick et al. 1993). SOLARFLUX utilizes the programming strategy of its predecessor, CANOPY (developed by Paul M. Rich in 1989), which analyzed whole sky images to quantify canopy and sky obstructions, and determined the solar radiation. The SOLARFLUX model output is a map with solar radiation values for a topographic surface. The output includes the total direct radiation, duration of direct sunlight, total diffuse radiation, sky view factor (ratio of diffuse sky irradiance to an unobstructed horizontal surface), and hemispherical "view sheds" of sky obstructions.* Based on the provided SOLARFLUX information, this model does not require input from an Internet resource (Rich et al. 1996).
- Geostationary Operational Environmental Satellite (GOES) Particle Filter (PF) Model: The GOES PF Model combines GOES satellite and surface

* View sheds are the elevation angles calculated when determining sky-view factors. They can be used by programs, such as CANOPY, to generate hemispherical views upward from a particular surface location.

observations. The observation function applies a particle filter method and a joint probability distribution. The model avoids complex radiative transfer equations by connecting the global and local dynamics of surface solar irradiance in a recursive Bayesian framework. Model input utilizes atmospheric composition data and pairs them with the solar geometry (solar zenith angle and direct solar contact). Through the GOES PF particle filter and observation function methods, high-quality surface solar irradiation estimations were produced over French Guinea with favorable results (Linguet and Atif 2015).

- Solargis Solar Model: The Solargis Solar Model is a semi-empirical model that determines solar irradiance from satellite data. The three-step design starts with a clear-sky model, from which Solargis calculates the clear-sky irradiance. GOES satellite data are used to quantify the attenuation effect of clouds via a cloud index calculation. Coupling the clear-sky irradiance with the cloud index, direct normal and global horizontal irradiance values are generated. These values are used in the last step, which calculates diffuse and global-tilted irradiances, and irradiance corrected for shading effects from surrounding terrain or objects. The model time and spatial resolutions are a function of the satellite data, which are 15–30 min and about 3 km (2 arc-minutes [about 4 × 4 km]). The atmospheric input parameters (water vapor and aerosols) represent daily data. Other input includes terrain shading, altitude, air temperature, solar geometry, and visible/IR satellite. Since this model requires an outside connection (to satellite data), its applicability to the project is limited (Solargis 2018).

- Bird Simple Spectral Model: The Bird Simple Spectral Model was developed by Richard Bird and Dr. Carol Riordan in the 1980s. This model computes clear-sky spectral direct-beam, hemispherical diffuse, and hemispherical total irradiances for a tilted or horizontal plane at a single point in time. The model input includes aerosol descriptors (ozone, total precipitable water vapor, etc.), solar geometry, surface pressure, and ground albedo. The output does not allow for any time varying parameters. This model had been tested for clear days only (Bird and Riordan 1984).

- American Society of Heating, Refrigeration and Air Conditioning (ASHRAE): The ASHRAE Clear Sky Model produces an hourly estimate of solar surface radiation under clear skies. Without clouds or aerosols, the solar radiation is a function of solar geometry and ground albedo. The model output includes hourly and monthly averaged estimates of the global, direct beam, and diffuse radiation. The model was tested against data acquired from a Kipp and Zonen CM-11 pyranometer at the Solar Energy Laboratory

in Aligarh, India. The three-day validation study reported root–mean–square errors of 0.2288 (2014 May 17), 0.0560 (2014 June 11) and 0.2001 (2014 July 08). Each of these cases generated the expected clear sky Gaussian curve (Besharat and Khan 2014).

- Solar Radiation Flux (SRF) Model: The SRF Model developed by Robert Shapiro will be described in the next section.

Table 1 Sample of surface solar radiation models

Model name	Model input	Model output	Networked resources required?
SOLARFLUX (also known as GIS Solar Flux Model)	Solar geometry, atmospheric attenuation, topography, horizon shading	Total direct and diffuse radiations, direct-sunlight duration, skyview factor, hemispherical view sheds	No
Geostationary Operational Environmental Satellite with Particle Filter (GOES PF) Model	Solar geometry, atmospheric composition, GOES satellite imagery	Surface solar irradiance	Yes
Solargis Solar Model	Solar geometry, atmospheric composition, GOES satellite images, environmental variables	Direct and horizontal diffuse solar irradiation	Yes
Bird Simple Spectral Model	Solar zenith angle, atmospheric turbidity, perceptible water	Single point in time, clear-sky spectral direct irradiance, diffuse and total irradiances	No
ASHRAE Solar Model	Solar geometry, ground albedo	Hourly/monthly estimates of global, direct beam, and diffuse solar radiation	No
Solar Radiation Flux Model	Solar geometry, local sky and environmental conditions	Local solar radiation	No

3.2 In-situ Solar Radiation Model Selection

The net result from the model surveys was the identification of a solar radiation model that was able to satisfy the key requirements for the tactical power grid environment. This model was the Solar Radiation Flux (SRF) Model, which was designed by Ralph Shapiro and published in 1982. The model's original application was for heat balance of terrestrial objects and backgrounds. The design was deliberately kept simple (quick processing) and constructed for applications with input solely from routine surface weather observations (input requires in-situ measurements only).

Research that led to the creation of the Shapiro SRF Model investigated and confirmed that the fraction of sunlight reflected, transmitted, and absorbed was proportional to the cloud type (i.e., cloud density and thickness). For example, Haurwitz (1948) was able to obtain estimates of mean transmissivity as a function of cloud type and solar zenith angle. His range of cloud types was limited, particularly at larger zenith angles. Shapiro was able to expand the restriction by using the SOLMET dataset. The dataset used Eppley bulb-type pyranometers, which had sensor aging issues. These data were processed so that only uniform sky states (all three layers clear; all three layers overcast) were used. With 13 weather stations across the continental United States, Shapiro inverted the reflection, transmission, and absorption model to calculate the coefficients. The data were processed by stations (hourly). Once satisfied that there were no geographical biases, Shapiro combined the results and subdivided them into uniform sky/weather conditions and cos zenith angle.

3.2.1 SRF Model Design

The SRF Model design assumes that

- The fraction of sunlight reflected, transmitted, and absorbed is the same for upward and downward fluxes.
- Fractions of reflected, transmitted, and absorbed radiation do not depend on incident flux direction.
- Solar radiation is quasi-monochromatic.
- *All* clouds are considered "thick", except for thin cirrus and cirrostratus.

The SRF Model uses plane-parallel homogeneous layers of arbitrary thickness. At the ground layer, transmission is 0. The radiation incident on a layer (k) is a closed system. That is, the fractions of reflected (R), transmitted (T), and absorbed (A) radiations equal 1 ($R_k + T_k + A_k = 1$) and do not depend on incident flux direction.

3.2.2 SRF Model Input/Output

The SRF Model input requires knowledge of reflection, transmission, and absorption for individual cloud types (summarized in tables), cloud amount, and cloud level. The default model input consists of three standard atmospheric layers reported by observers: low (0–2 km), middle (2–7 km), and high (7–10 km). Reflectivity, transmissivity, and absorptivity coefficients for each plane-parallel atmospheric layer are a function of time and space, as previously explained. The choice for three layers provides good first approximations, though additional layers are possible. Shapiro noted that if layers were thin enough the coefficients could be constant for that layer, time, and location (Shapiro 1982).

The SRF Model output consists of solar radiation (direct and diffuse) received at the ground. Direct radiation in the SRF Model is defined as solar radiation transmitted through a layer with < 7/8 thick clouds; diffuse radiation is defined as radiation transmitted through a layer with $\geq$ 7/8 thick clouds.

3.3 Data Preparation for Model Input Requirements

For the SRF Model to automatically provide the surface solar radiation, in-situ observations are needed. Using a whole sky imager would be good but not tactical. Consequently, an sWSI was pursued. As explained earlier, the ARE field studies included imagery from sWSI. Recapping the earlier description, the sWSI consisted of a Professional Nikon D750 camera fisheye lens. Applying skillful exposure techniques (Vaucher et al. 2017), details of sky and clouds were preserved on the digital film, despite the inclusion of direct sunlight. These hourly images were manually acquired between 0800 and 1600 Mountain Daylight Time, during most ARE Field Study business days. An observer documented sky conditions within minutes of the sWSI data acquisition. As per model requirements, the observer subdivided the description into three layers (low, middle, and high cloud), nine cloud types, and estimated amounts (in tenths). The US Navy's *Aerographer's Mate Third Class (Observer)* manual and the National Oceanic and Atmospheric Administration (NOAA)—NASA cloud standards defined the cloud layer and types (NETPDC 1984; NWS 2015). For more information, see Vaucher et al. (2017). These observations were supplemented by online, automated observations from an Air Force base that was about 40 miles east–northeast of the ARE site.

3.3.1 sWSI Data Preparation

Each sWSI image was manually prepared for machine learning applications. That is, a grid was overlaid onto the image and numerical codes were assigned that described the features within the grid box. The main function of the code was to

distinguish between lens artifacts and valuable sky information. Examples of the features include All Clouds, All Clear, Partial Cloud/Sky, Image Border with All Clouds/Clear Sky/Partial Cloud-Sky, Sun Glint, Sun and Glory with All Clouds/Clear Sky/Partial Cloud-Sky, or the background Black Border. Figure 3 shows a generic example of the digitized image results. (Note: The image analysis was not a function of pixel type.)

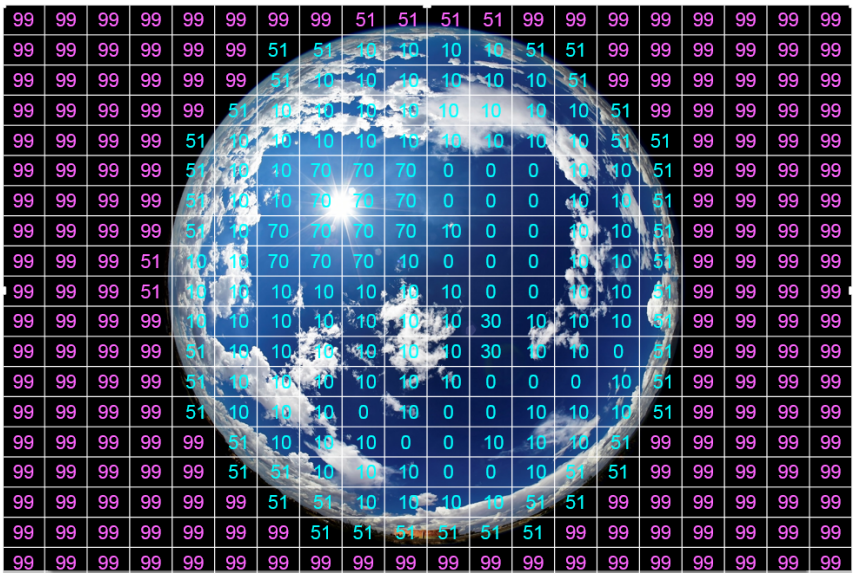

Fig. 3 Generic sWSI digitization example (Vaucher et al. 2017)

3.3.2 ARE3 sWSI Observations and Comments

While digitizing/analyzing the sWSI images, some common characteristics and trends were noted by the analyst. These included the following:

- On clear days, the angled sWSI images generally had sharper borders and sky; the zenith sWSI images captured more haze around the perimeter of the image, especially along the eastern half.*
- On clear days, more sun glory and photo artifacts were observed.
- On overcast or partly cloudy days, there were fewer observable small artifacts.
- On rainy days, the water droplets on the sWSI lens were part of the photo.
- To reduce lens artifacts, it is important to keep the lens clear of any dust, dirt, or finger oils.

* The angled camera (perpendicular to the sun rays) had less sky data, since it captured more of the local physical structures than the zenith camera.

Appendix A reviews the former ARE2 sWSI "Observations and Comments".

4. Discussion—ARE3 Preliminary Results

While Section 3 focused on preparing the SRF Model input, a review of the ARE3 data has provided additional insights into the relationships between solar radiation and power generation. A sample follows, beginning with the alignment of the time stamp, and the relationship between the three power measurements. An observed graphical correlation between solar input and a power grid "in" and "out" of balance follows. For additional data review, graphical representations of the daily ARE3 Power Train and Pyranometer data are shown in Appendices B and C, respectively.

4.1 Time Stamp Alignment

Power and atmospheric data from ARE3 were aligned through a GPS-derived time stamp, which was checked and calibrated daily during both the ARE2 and ARE3 field studies. This parameter was a critical prerequisite to the data analyses. A summary of the ARE3 alignment process follows.

Each field study day began with a time calibration/validation for the power, pyranometer, and sWSI data acquisition systems. The "true" time stamp originated from the Nikon GP-1, a GPS device attached to the sWSI. Once locked in, the sWSI time stamp display was used to update both the Pyranometer CR6 data logger and the associated Inspiron Data Acquisition System (DAS) archive time stamps. Time values observed and/or changed were documented in the ARE field logbooks. If a time difference of more than 5 s was noted, the CR6 time was resynchronized with the GPS-calibrated Inspiron clock and the update was noted in the logbook. The Labview–Power Train DAS program copied its time stamp from the resident DAS computer, which was automatically updated using a second GPS device. A comparison between DAS clocks (Pyranometer/Inspiron and Power/Labview) was noted and logged.

4.2 Power Data Checks

As with ARE2, a daily inspection of the ARE3 data acquired produced midnight to midnight time series plots, such as those shown in Fig. 4. In Fig 4a, the three pyranometers indicate an acceptable agreement under mostly cloudy skies in the late morning–early afternoon (noted by the jagged time series) and clearer skies in the mid-to-late afternoon (noted by the smooth curves). The Power Train plots not only showed the three power samples, but compared the net difference between the PV generated power minus the sum of the Battery and Load Powers. In Fig. 4b, the

combined battery and load values are shown by the dark green "x". While visually close to the PV power, a calculated difference is presented by the gray dashed time series. For this July 28 case, the average differential was 4.376 W/m^2, having a maximum value of 12.346 W/m^2 and minimum of 1.671 W/m^2. July 28 was chosen to demonstrate the effects of a clear sky (late afternoon: 1600–1900 local time [LT]) versus the slightly higher and "noisier" power differences during the mostly cloudy time periods (1100–1300 LT).

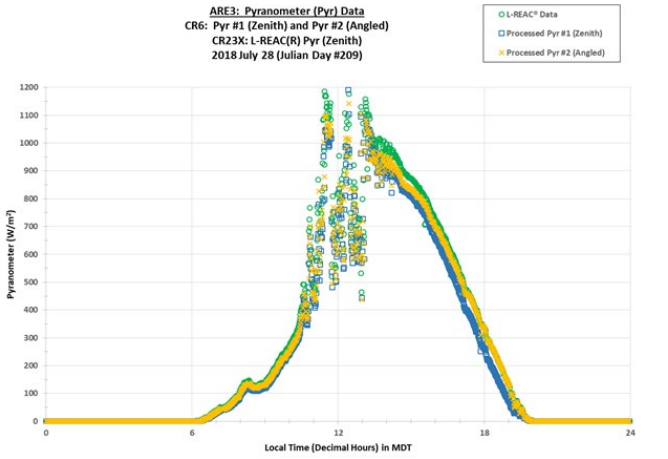

a)

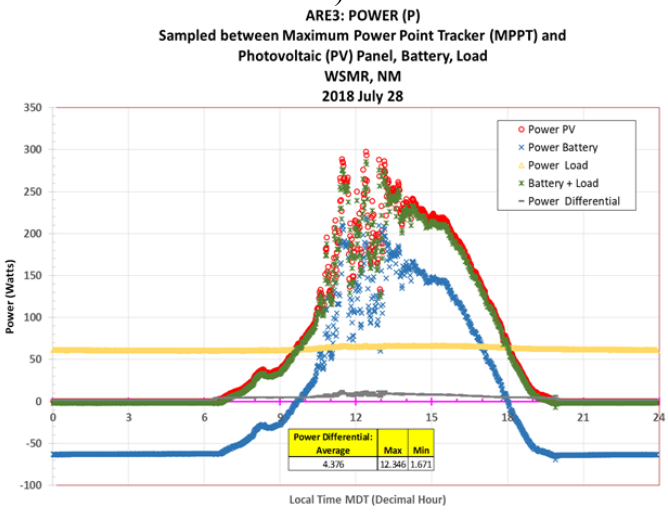

b)

Fig. 4 ARE3 2018 July 28 data. a) Pyranometer (surface solar radiation) data: the jagged time series between 1100 and 1300 LT stems from clouds occulting the sun, whereas the smooth late afternoon solar radiation curve indicates clear skies (1600–1900 LT), b) Power Train data: the differential between PV Power and "Battery + Load" summation Power is shown in gray; slightly higher and "noisier" gray power differentials were observed 1100–1300 LT, a mostly cloudy period.

4.3 Power and Pyranometer Data Trends

Optimizing a hybridized power grid that includes solar energy requires knowledge of current and future atmospheric conditions. The application of the atmospheric information is not to enable the replacement of all of the diesel generators, but more to optimize the traditional generators' performance (maximizing fuel economy) and minimize the need for secondary resources to cover load spikes—in short, creating a "balanced" power grid.

In the course of analyzing the ARE3 data, two distinctive power time-series patterns contrasted a balanced and unbalanced (wasted energy) power train. Consider the three power plots from July 24 (Fig. 5) and July 26 (Fig. 6). These figures show the local midnight-to-midnight time series for a) voltage, b) current, and c) power. The first observation is that the Power time series largely imitates the graphical shape of the Current. This trend was consistent whether the power system was in or out of balance.

Unbalanced Grid: On July 24 the load was digitally set to 0.5A. The power draw was extremely low with respect to the abundant solar power being generated. Consequently, the MPPT utilized a bulk energy transfer to charge the batteries until the batteries were full. A forced shedding of subsequent energy dissipated the excess power generated. The sharp split in the time series around 1200 LT shows where the power-distribution method shifted from "a bulk" to "a floating" distribution. This floating ("topping off" of the battery) method persisted until the sunset (D'Arcy 2018).

Balanced Grid: On July 25 the Load was manually increased from 0.5A to 3A at 1100 LT. While the bulk and floating power distributions continued for the remainder of July 25, the Power distribution had finally balanced by July 26 (Fig. 6). In the July 26 Power Train plots, the graphical shape of the Current and Power curves continues to be similar. Of note, however, is that the graphical shape is also similar to the incoming solar radiation as measured by the pyranometer. For as long as the Power remained "balanced", the Current, Power, and Solar Radiation curves followed the same general magnitude shifts. This "balanced" pattern persisted for the remainder of the ARE3 sampling sessions.

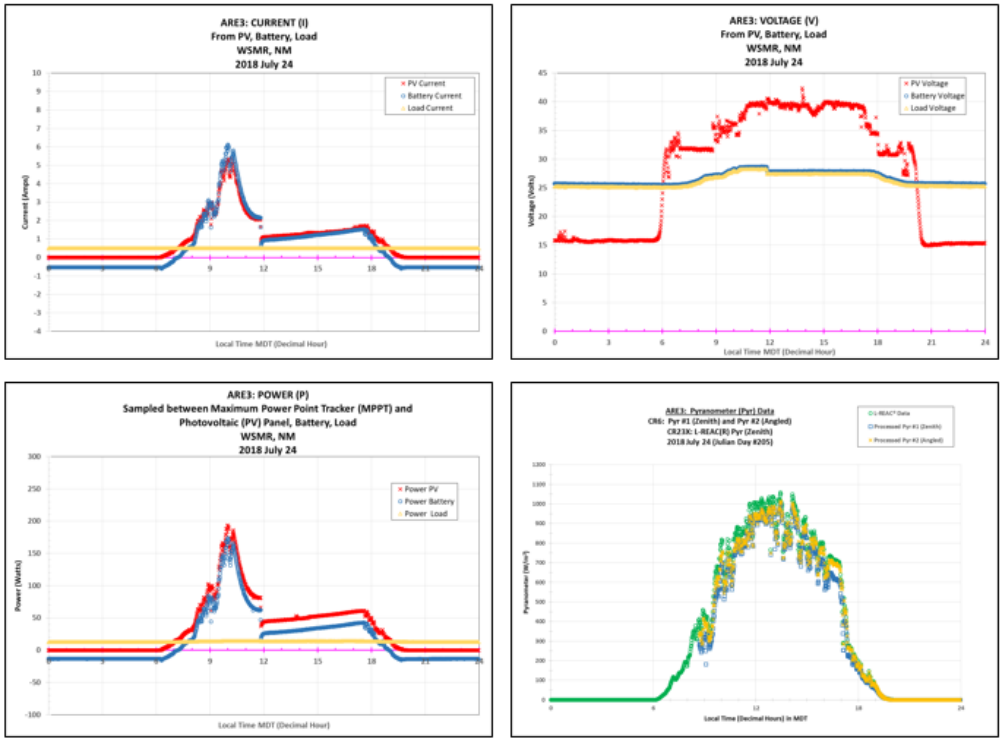

Fig. 5 Unbalanced power grid: 2018 July 24—ARE3 Current, Voltage, Power, and Pyranometer (surface solar radiation) time series

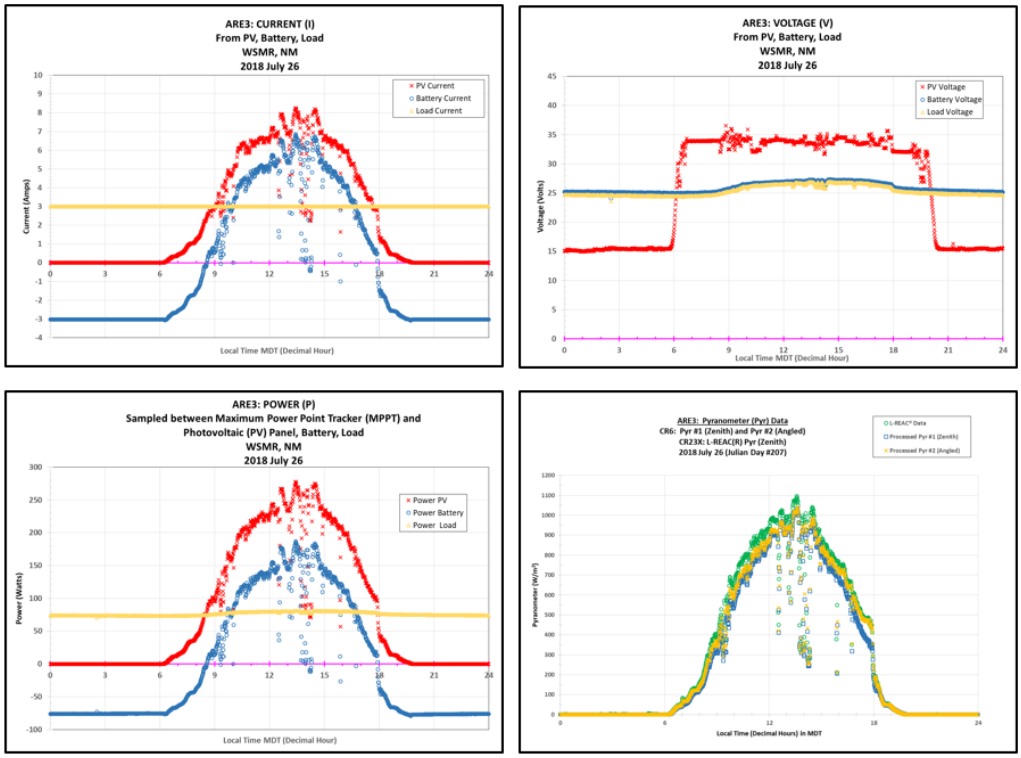

Fig. 6 Balanced power grid: 2018 July 26—ARE3 Current, Voltage, Power, and Pyranometer (surface solar radiation) time series

5. Conclusion and Recommendations

The ARE3 field study documented in this report has furthered the acquisition of novel and detailed power and atmospheric data. These data serve as important resources toward the development of a solar radiation flux model that will provide atmospheric intelligence for future tactical power grids. A sample of solar radiation models surveyed for hybrid power applications was presented, along with the identification of a "best fit" model that satisfies the baseline requirements for tactical energy unit independence. Supplementing the investigation, the ARE3 data provided updated Power Train analyses and examples of balanced and unbalanced power grids. In summary, with the acquired ARE3 data and this report, ARL continues to advance toward a better understanding of the atmospheric influences upon the hybrid power grids utilizing solar energy, as well as to make valuable progress toward the creation of a smart (atmospherically informed) tactical hybrid power grid.

6. References

[AMS] American Meteorological Society. Meteorology glossary; 2012 [accessed 2018 Sep 11]. http://glossary.ametsoc.org/wiki/Pyranometer.

Auligné T. Multivariate minimum residual method for cloud retrieval. Part I: theoretical aspects and simulated observations experiments. Mon Wea Rev. 2014a;142:4383–4398.

Auligné T. Multivariate minimum residual method for cloud retrieval. Part II: real observations experiments. Mon Wea Rev. 2014b;142:4399–4415.

Besharat J, Khan M. Estimation of clear-sky solar radiation using ASHRAE model for Aligarh, India. Int J Eng Res Tech. 2014;7(3):227–236.

Boxwell M. Solar electricity handbook, 2013 edition: a simple, practical guide to solar energy–designing and installing photovoltaic solar electric systems. Ryton on Dunsmore Warwickshire (UK): Greenstream Publishing; 2013.

Bird RE, Riordan C. Bird simple spectral model. National Renewable Energy Laboratory (US); 1984 [accessed 2018 Aug 08]. https://www.nrel.gov/grid/solar-resource/ spectral.html.

D'Arcy S. Computational and Information Sciences Directorate, White Sands Missile Range, NM. Personal communication, 2018 July 26.

Descombes G, Auligné T, Lin HC, Xu D, Schwartz C, Vandenberghe F. Multi-sensor advection diffusion nowCast (MADCast) for cloud analysis and short-term prediction. Boulder (CO): National Center for Atmospheric Research (US); 2014 July. Report No.: NCAR/TN-509+STR.

[DOD] Department of Defense. Directive 4180.01: DoD energy policy. Washington (DC): Department of Defense (US); 2014 Apr 16.

Haupt SE, Branko K, Jensen T, Lee J, Jimenez P, Lazo J, Cowie J, McCandless T, Pearson J, Weiner G, et al. The SunCast solar-power forecasting system: the results of the public-private-academic partnership to advance solar power forecasting. Boulder (CO): National Center for Atmospheric Research, Research Applications Laboratory, Weather Systems and Assessment Program (US); 2016 Jan. Report No.: NCAR/TN-562+STR.

Haurwitz B. Insolation in relation to cloud type. J Meteor. 1948;5:110–113.

Hetrick WA, Rich PM, Barnes FJ, Weiss SB. GIS-Based Solar radiation flux models. American Society for Photogrammetry and Remote Sensing Technical Papers. Vol 3, GIS. Photogram Model. 1993;3:132–143.

Linguet L, Atif J. Estimating surface solar irradiance from GOES satellite with particle filter model and joint probability distribution. Canadian J Rep Sen. 2015;41(2):71–85.

[NETPDC] Aerographer's Mate Third Class (Observer), Naval Education and Training Command, rate training manual and nonresident career course. Pensacola (FL): Naval Education and Training Program Development Center (US); 1984.

[NWS] NOAA/NWS and NASA sky watcher chart. Silver Spring (MD): National Weather Service; 2015 [accessed 2017 Oct 27]. https://www.weather.gov/media/owlie/skywatchers_chart.pdf.

Parker G. Michigan Technology University, Houghton, MI. Personal communication, 2018 May 30.

Rich PM. Hetrick WA, Saving SC. Modeling topographic influences on solar radiation: a manual for the SOLARFLUX model. National Energy Technology Laboratory: Department of Energy (US); 1996 [accessed 2018 Aug 07]. https://www.osti.gov/biblio/200698.

Shapiro R. Solar radiative flux calculations from standard surface meteorological observations. Air Force Geophysics Laboratory (MA): Air Force Systems Command (US); 1982 Mar. Report No.: AFGL-TR-82-0039.

Solargis. Methodology–solar radiation modeling; 2018 [accessed 2018 Aug 7]. https://solargis.com/docs/methodology/solar-radiation-modeling/.

[US Congress] United States Congress. Public Law 109–58. Energy policy act of 2005. Washington (DC): Government Printing Office (US). 2005 Aug 8.

Vaucher G. Atmospheric renewable-energy research, volume 1. White Sands Missile Range (NM): Army Research Laboratory (US); 2015 Sep. Report No.: ARL-TR-7402.

Vaucher G. Atmospheric renewable energy research, volume 2: assessment process for solar-powered meteorological applications. White Sands Missile Range (NM): Army Research Laboratory (US); 2016 Aug. Report No.: ARL-TR-7762.

Vaucher G, Smith J, Berman M. Atmospheric renewable energy research, volume 3: solar-power microgrids and atmospheric influences. White Sands Missile Range (NM): Army Research Laboratory (US); 2016 Sep. Report No.: ARL-TR-7797.

Vaucher G, Forrester J, Curtice, M, Young R, Walker C, D'Arcy S. Atmospheric renewable energy research, volume 4: atmospheric renewable energy field study #2 (ARE2). White Sands Missile Range (NM): Army Research Laboratory (US); 2017 Oct. Report No.: ARL-TR-8189.

Walker C, Vaucher G. Atmospheric renewable energy research, volume 5 (solar radiation flux model). White Sands Missile Range (NM): Army Research Laboratory (US); 2017 Sep. Report No.: ARL-TR-8155.

Appendix A. Atmospheric Renewable Energy Field Study No. 2 (ARE2) Comments and Observations

The 2017 ARE2 field study included approximately 10 weeks of routine, hourly cloud observations along with a manual evaluation of the ARE2's simulated Whole Sky Imager (sWSI) images for lens artifacts versus sky data. The ARE2 participants' observations and lessons learned documented by Vaucher et al. (2017)[†] are reviewed here, as a supplement to the 2018 ARE3 observations:

1) Automating the sWSI Image Analyses: The sWSI image analyses are not a function of just the pixel type (red, green, or blue); it is the interpretation of what sky or lens feature is represented by the pixel that is the goal. This added discriminatory layer is what keeps a human in the loop for this step of the post-processing. With enough digitized data input, however, it is hoped that machine learning will ultimately reduce the need for, or perhaps even replace, the human in the loop.

2) Analysis challenges: There were instances when lens artifacts overlapped within the same grid cell. For example, lens glint and U-Glow would overlap, or the sun overlapped with the border, or the sun overlapped with the glint. On a cloudy day, clouds and glint might overlap. There should be a special description for these situations.

3) Lens artifacts (optical effects):

    a) Lens flare and abnormal light areas in an image are caused by repeated reflections off of optical surfaces in the lens, with air spaces in between the lens elements. Light that encounters such surfaces will refract through the lens and reflect off the surfaces of subsequent elements, which reduces the amount of light that gets transmitted through the next element.

    b) Lens flare is minimized when you multicoat all optical surfaces within the lens, which is composed of elements separated by air spaces. Such multicoating increases the refraction of light through the lens element and decreases the reflection off that same surface, thus decreasing the flare. A perfect multicoated lens will not produce flare.

    c) A sun star is caused by light interacting with the rough/angled edges of the iris blades (of the F-stop diaphragm). To minimize the effect, the lens should have an increased number of diaphragm blades and be curved so that a perfect iris circle is made at all F-stops. The more

[1] Vaucher G, Forrester J, Curtice, M, Young R, Walker C, D'Arcy S. Atmospheric renewable energy research, volume 4: atmospheric renewable energy field study #2 (ARE2). White Sands Missile Range (NM): Army Research Laboratory (US); 2017 Oct. Report No.: ARL-TR-8198.

circular the iris is, without rough edges between blades, the less points to the sun star. A perfect circle resolves into no sun star. A 10-pointed star comes from a 5-bladed diaphragm. One can count the number of sun-star points to figure out the number of blades in the optics diaphragm.

d) The shape of the lens flare (such as a pentagon) can also tell you how many diaphragm blades there are (and vice versa).

Observations from the sWSI data preparation and analyses follow:

Climatological observations:

- ARE2 seasonal cases confirmed: In June 2017 there were little to no clouds in the sky. When the monsoon arrived in July 2017, clouds of various types populated the New Mexico sky.
- ARE2 overcast case studies: Some July morning skies started as overcast, which could be good post-ARE2 case-study material.
- ARE2 cumulus (Cu) case studies:
    - In June, the Cu clouds did not have much buildup. The buildup started to occur in July. There were numerous cumulonimbus clouds during July. A few occurred directly over the site.
    - In June, July, and August, Cu clouds repeatedly developed on the eastern horizon, near the tallest-peak mountains.
    - In July, Cu clouds frequently formed over southwestern mountains.

ARE2 haze: Near-surface haze cases were difficult to discern from just the post-processing images.

ARE2 lens artifacts:

- Solar disc: When the sun was close to the horizons (morning and evening time periods), the solar disc appeared relatively small with respect to the solar disc seen during the midday hours.
- Sun and lens glint: The locations of the sun and lens glint followed a distinct pattern. During the morning and evening hours, the sun and glint were far from each another. When the sun was on the eastern horizon, the glint was observed in the western part of the field of view. By 1600 local time (LT), as the sun was approaching the western horizon, the glint was near the

eastern horizon. During the midday hours, the sun and glint moved closer together, overlapping at 1300 LT.

- Sun glint and U-glow ("array of the sun"): A "U-glow" is an artifact of the fisheye lens that causes the sunlight to glow in a semicircle. The U-glow generally only appeared between 1100 and 1600 LT. The glint and U-glow had a relationship in that they were always opposite one another. The U-glow generally initiated on the east side of the sun, while the glint was on the west side. When the U-glow was observed on the west side of the sun, the glint would be on the east side. If the glint position was southwest of the sun, the U-glow would be northeast of the sun.
- Lens reflection: In some of the 0800 LT, west-pyranometer platform images, a reflection appeared lower than the horizon. This reflection was only present during the morning hours, when the sun was close to the horizon. As soon as the sun gained elevation (approximately 0900 Mountain Daylight Time), the reflection disappeared.

Appendix B. Atmospheric Renewable Energy Field Study No. 3 (ARE3) Power Data

The following 2018 ARE3 Power plots show a daily (local midnight-to-midnight) time series for the three "balanced" Power types sampled. The PV Power (sampled between the PV and Controller) is labeled with a red circle; Battery Power is displayed with a blue x; and Load Power is shown with a yellow triangle. The "Battery + Load" sum is plotted with a green star, while the Power differential between PV power and "Battery + Load" sum is shown by a gray hyphen. The average, maximum and minimum power differentials are noted on the plot.

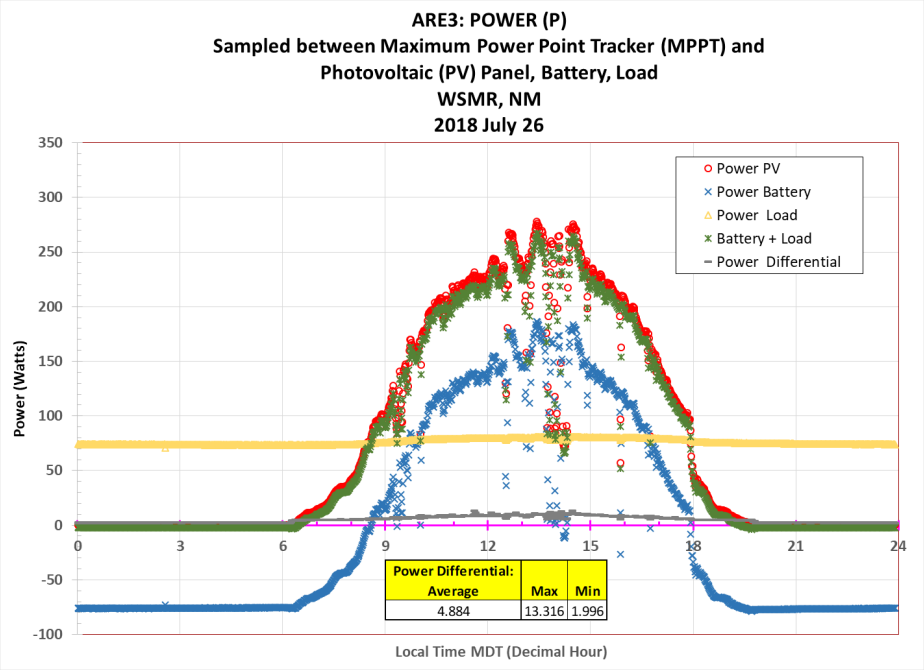

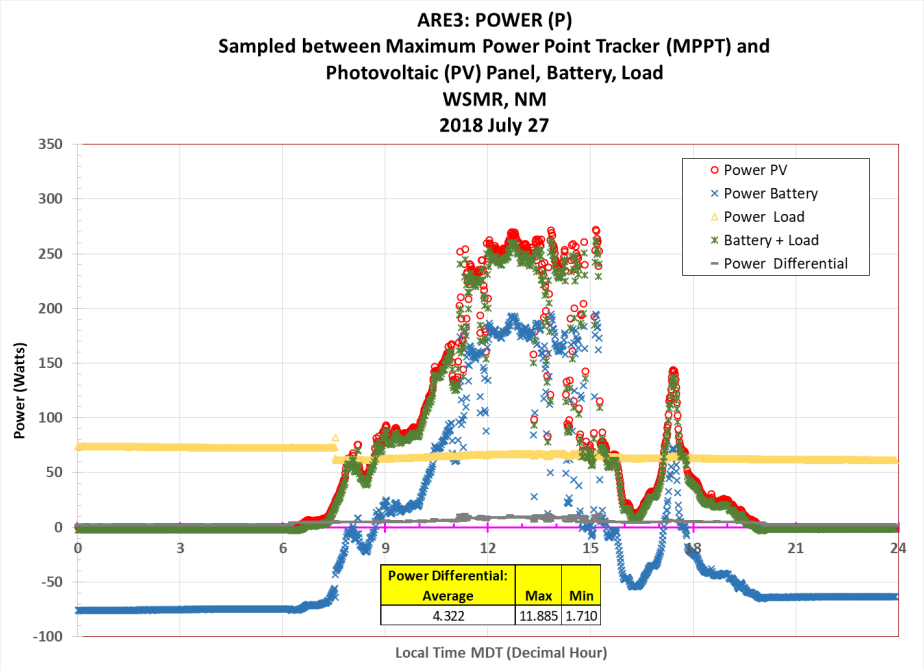

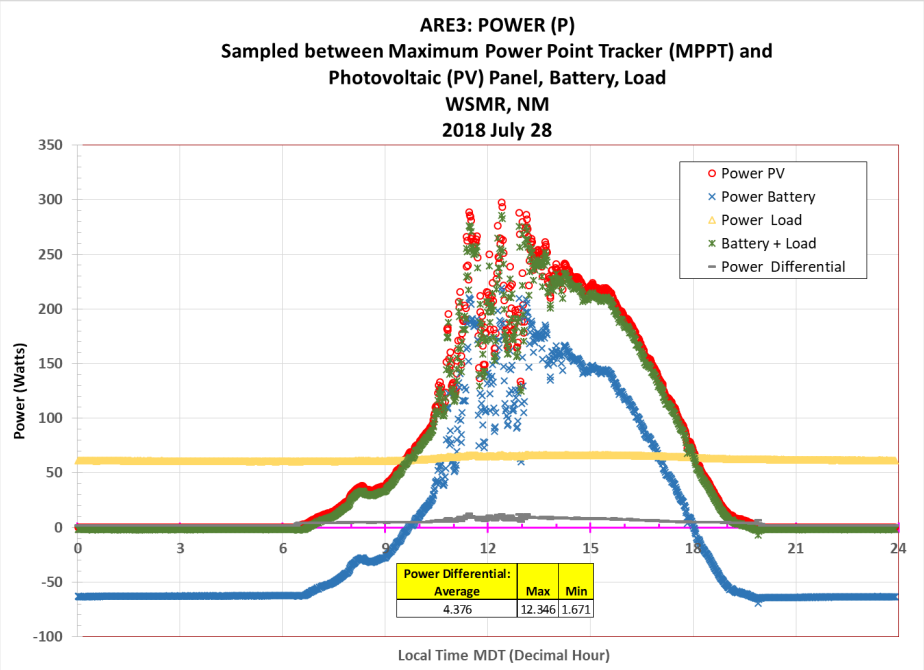
ARE3: POWER (P)
Sampled between Maximum Power Point Tracker (MPPT) and
Photovoltaic (PV) Panel, Battery, Load
WSMR, NM
2018 July 28
Power PV
Power Battery
Power Load
Battery + Load
Power Differential
Power (Watts)
Local Time MDT (Decimal Hour)
Power Differential: Average
Max
Min
4.376
12.346
1.671

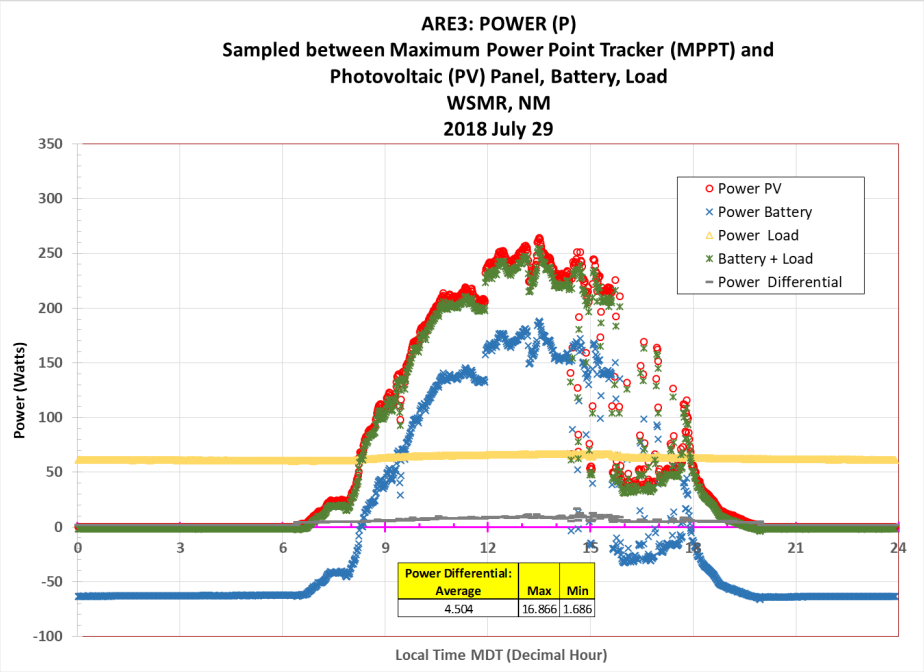
ARE3: POWER (P)
Sampled between Maximum Power Point Tracker (MPPT) and
Photovoltaic (PV) Panel, Battery, Load
WSMR, NM
2018 July 29
Power PV
Power Battery
Power Load
Battery + Load
Power Differential
Power (Watts)
Local Time MDT (Decimal Hour)
Power Differential: Average
Max
Min
4.504
16.866
1.686

Appendix C. Atmospheric Renewable Energy Field Study No. 3 (ARE3) Pyranometer Data

The following 2018 ARE3 Pyranometer data include coincident data from the Local-Rapid Evaluation of Atmospheric Conditions (L-REAC) System, along with the zenith and angled pyranometers attached to the ARE3 photovoltaic panel. The first six plots present daily time series (local midnight to midnight); the final plot extends the solar radiation time series over the entire ARE3 time period, using a decimal Julian Day as the major time reference.

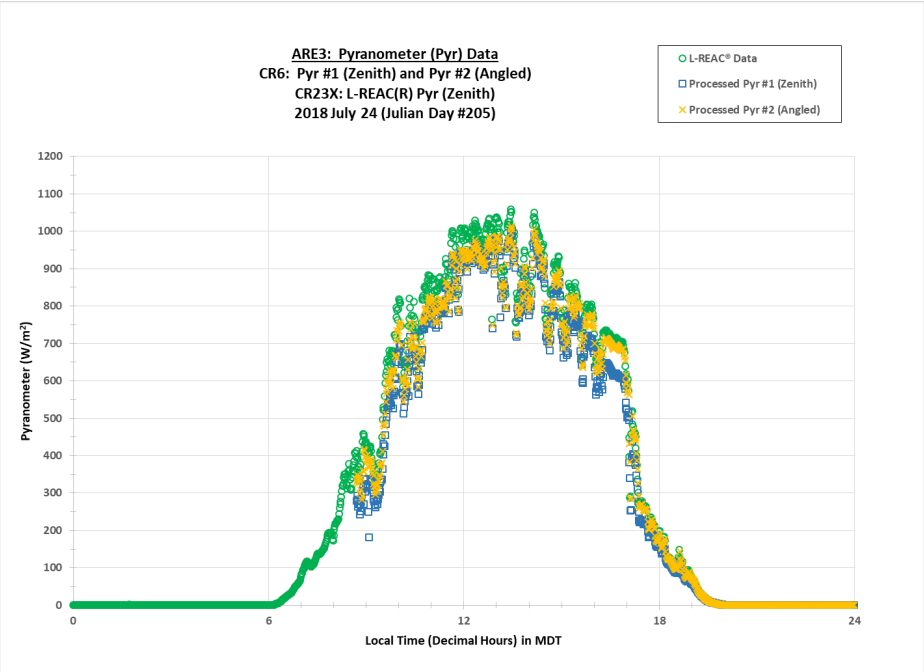

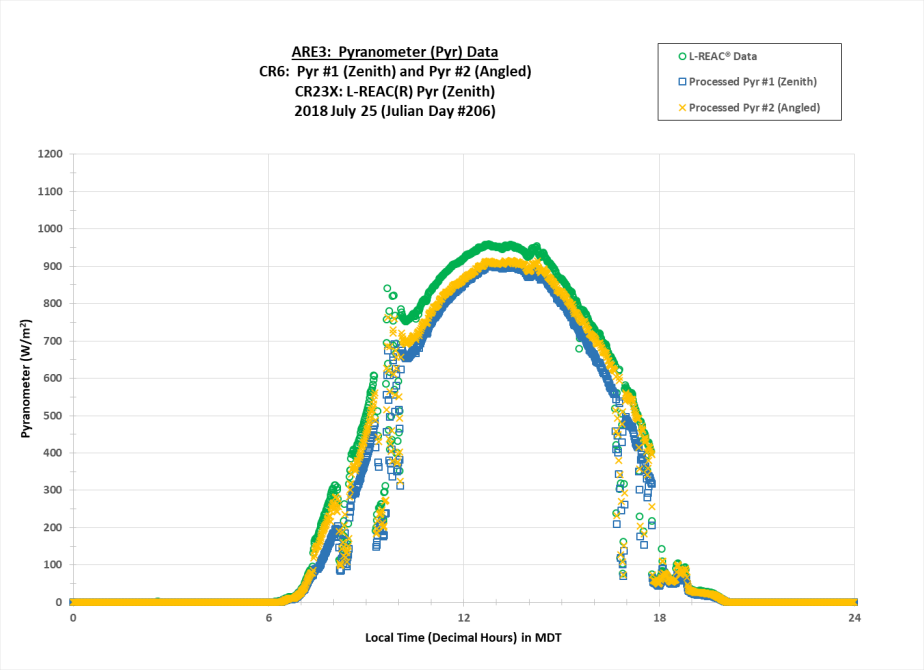

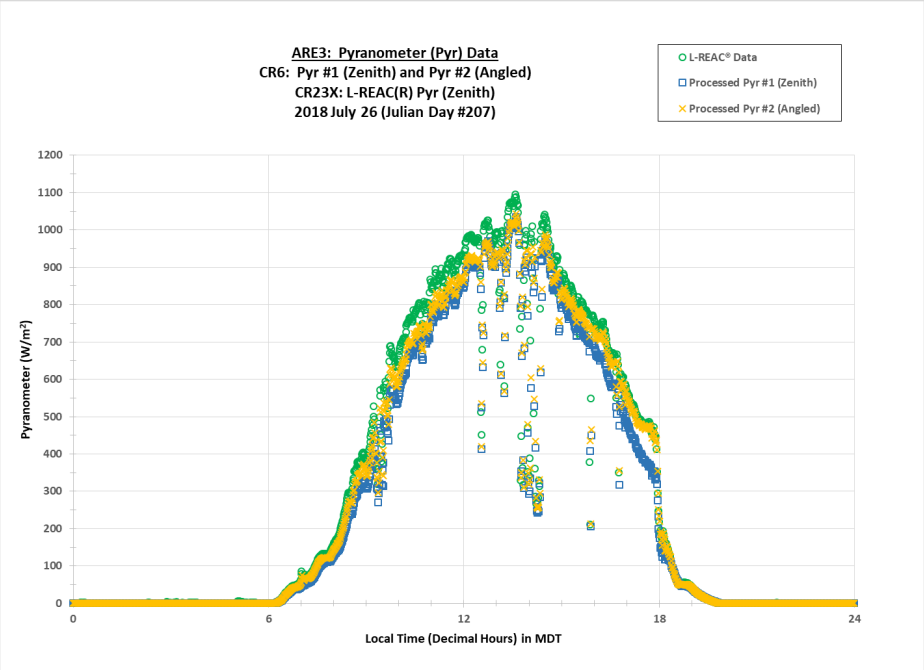
ARE3: Pyranometer (Pyr) Data
CR6: Pyr #1 (Zenith) and Pyr #2 (Angled)
CR23X: L-REAC(R) Pyr (Zenith)
2018 July 26 (Julian Day #207)
L-REAC® Data
Processed Pyr #1 (Zenith)
Processed Pyr #2 (Angled)
Pyranometer (W/m²)
Local Time (Decimal Hours) in MDT

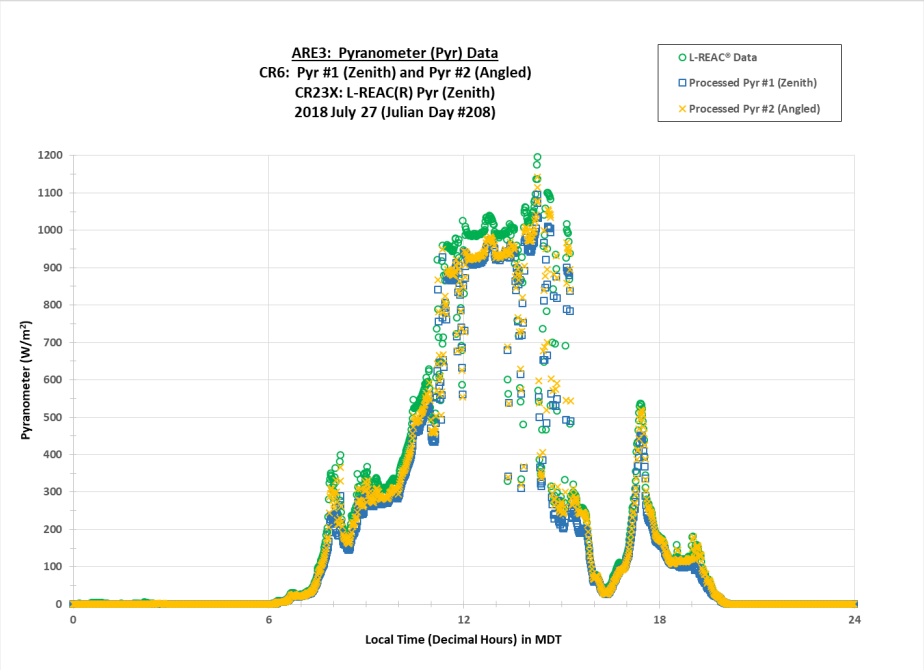
ARE3: Pyranometer (Pyr) Data
CR6: Pyr #1 (Zenith) and Pyr #2 (Angled)
CR23X: L-REAC(R) Pyr (Zenith)
2018 July 27 (Julian Day #208)
L-REAC® Data
Processed Pyr #1 (Zenith)
Processed Pyr #2 (Angled)
Pyranometer (W/m²)
Local Time (Decimal Hours) in MDT

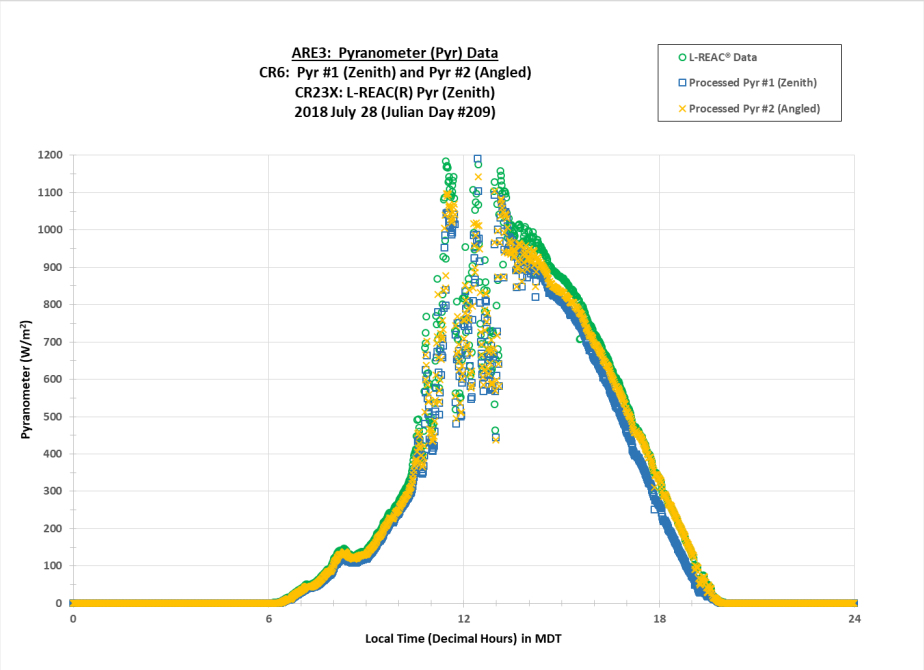
ARE3: Pyranometer (Pyr) Data
CR6: Pyr #1 (Zenith) and Pyr #2 (Angled)
CR23X: L-REAC(R) Pyr (Zenith)
2018 July 28 (Julian Day #209)
L-REAC® Data
Processed Pyr #1 (Zenith)
Processed Pyr #2 (Angled)
Pyranometer (W/m²)
Local Time (Decimal Hours) in MDT

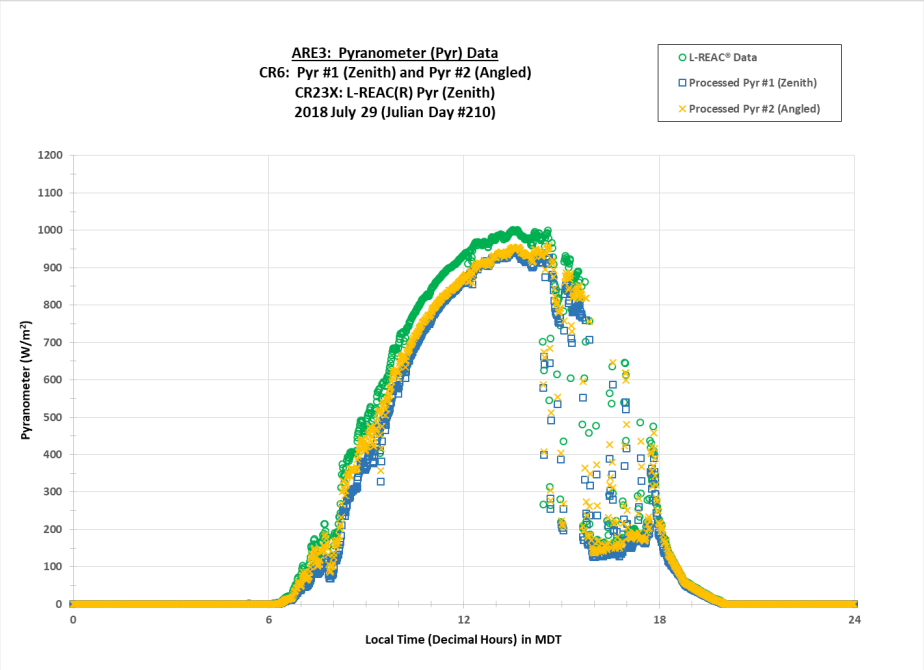
ARE3: Pyranometer (Pyr) Data
CR6: Pyr #1 (Zenith) and Pyr #2 (Angled)
CR23X: L-REAC(R) Pyr (Zenith)
2018 July 29 (Julian Day #210)
L-REAC® Data
Processed Pyr #1 (Zenith)
Processed Pyr #2 (Angled)
Pyranometer (W/m²)
Local Time (Decimal Hours) in MDT

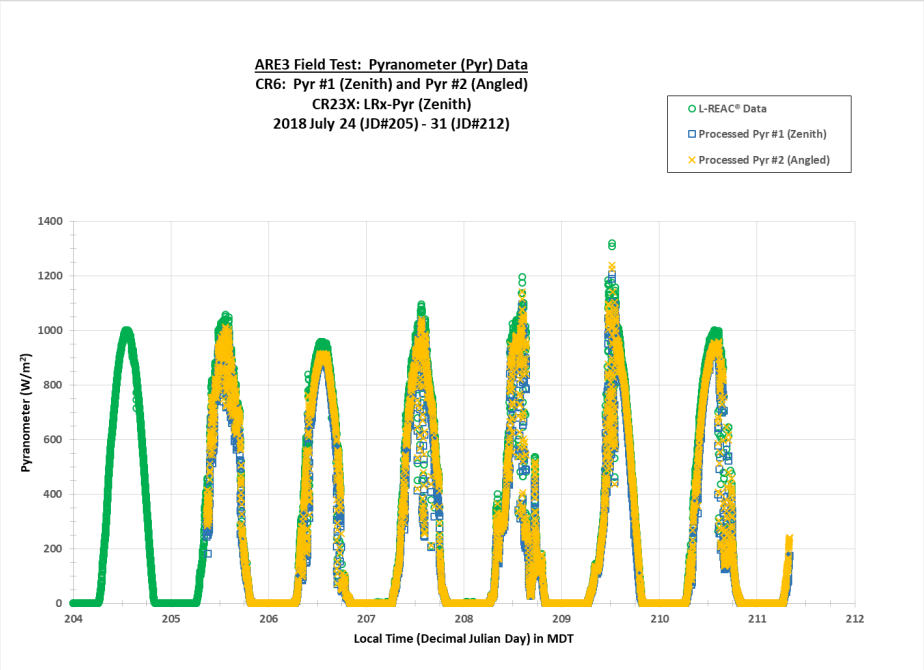
ARE3 Field Test: Pyranometer (Pyr) Data
CR6: Pyr #1 (Zenith) and Pyr #2 (Angled)
CR23X: LRx-Pyr (Zenith)
2018 July 24 (JD#205) - 31 (JD#212)
L-REAC® Data
Processed Pyr #1 (Zenith)
Processed Pyr #2 (Angled)
Pyranometer (W/m²)
1400
1200
1000
800
600
400
200
0
204
205
206
207
208
209
210
211
212
Local Time (Decimal Julian Day) in MDT

List of Symbols, Abbreviations, and Acronyms

3-D	3-dimensional
A	ampere
A	absorption
ARE	Atmospheric Renewable Energy
ARE2	Atmospheric Renewable Energy Field Study no. 2
ARE3	Atmospheric Renewable Energy Field Study no. 3
ArL	above roof level
ARL	US Army Research Laboratory
ASHRAE	American Society of Heating, Refrigeration and Air Conditioning
CIRACast	Cooperative Institute for Research in the Atmosphere Forecast
Cu	cumulus
DAS	Data Acquisition System
DC	direct current
DOD	Department of Defense
GIS	Geographic Information System
GOES	Geostationary Operational Environmental Satellite
GPS	global positioning system
L-REAC	Local-Rapid Evaluation of Atmospheric Conditions
LT	local time
MADCast	Multisensor Advection–Diffusion NowCast
MPPT	Maximum Power Point Tracking
MSL	mean sea level
NASA	National Aeronautics and Space Administration
NOAA	National Oceanic and Atmospheric Administration
PF	Particle Filter
PV	photovoltaic

R	reflectivity
SRF	Solar Radiation Flux
sWSI	simulated Whole Sky Imager
T	transmission
TSICast	Total Sky Imager Forecast model
V	voltage
W	watts
Wp	Peak Watts
WRF	Weather Research and Forecasting

1 (PDF)	DEFENSE TECHNICAL INFORMATION CTR DTIC OCA
2 (PDF)	DIR ARL IMAL HRA RECORDS MGMT RDRL DCL TECH LIB
17 (7 PDF, 5 HC, 5 CD)	ARL RDRL CIE D G VAUCHER (5 CD, 5 HC) S DARCY C HOCUT R RANDALL RDRL SED P M BERMAN D PORSCHET S HU
1 (PDF)	UNIV OF NEVADA RENO A WELCH